Correlation between Active Center Structure and Enhanced Dioxygen Binding in Co(salen) Nanoparticles: Characterization by In Situ Infrared, Raman, and X-ray Absorption Spectroscopies

Chad Johnson,[†] Brandon Long,[†] Joseph G. Nguyen,[‡] Victor W. Day,[‡] A. S. Borovik,[§] Bala Subramaniam,[†] and Javier Guzman*,[†]

Center for Environmentally Beneficial Catalysis and Department of Chemical and Petroleum Engineering, University of Kansas, Lawrence, Kansas 66045, Department of Chemistry, University of Kansas, Lawrence, Kansas 66045, and Department of Chemistry, University of California, Irvine, California 92697

Received: May 6, 2008; Revised Manuscript Received: May 30, 2008

The structure and ligand environment of Co(salen) nanoparticles and unprocessed Co(salen) have been determined by the combined application of infrared, Raman, X-ray absorption near edge structure (XANES), and extended X-ray absorption fine structure (EXAFS) spectroscopies, and X-ray diffraction (XRD) experiments before and during interaction with O_2. The Co(salen) nanoparticles were prepared by the precipitation with compressed antisolvent (PCA) technique using commercially obtained Co(salen) [denoted as unprocessed Co(salen)] as the parent compound. The unprocessed Co(salen) particles exist as dimer species with a square-pyramidal coordination geometry that display no measurable O_2 binding at room temperature. In sharp contrast, the Co(salen) nanoparticles show near-stoichiometric O_2 adsorption, as demonstrated by microbalance gas binding experiments. The spectroscopy results indicate the presence of Co^{II} centers with distorted tetrahedral geometry in the Co(salen) nanoparticles with no evidence of metallic Co clusters, confirmed by the lack of Co−Co contributions at bonding distances in the EXAFS spectra and the presence of characteristic features of Co^{II} in the XANES spectra. The EXAFS data also indicate that there are on average two Co−N and two Co−O bonds with a distance of 1.81 ± 0.02 and 1.90 ± 0.02 Å, respectively, consistent with typical metal salen structures. Upon O_2 binding on the Co(salen) nanoparticles, the XANES results indicate oxidation of the Co^{II} to Co^{III}, consistent with the vibrational data showing new bands associated with oxygen species bonded to Co centers and the increase in the oxygen coordination number from 1.8 to 2.9 in the EXAFS data. The results indicate that the enhanced O_2 binding properties of Co(salen) nanoparticles are related to the unique distorted tetrahedral geometry, which is not observed in the unprocessed samples that contain mainly dimers with square planar geometry. The results presented here provide a fundamental relationship between active center structure and properties of novel molecule-based nanomaterials.

Introduction

Nanomaterials with novel size-dependent properties and potential applications for catalysis, gas storage, and controlled release formulations are increasingly emerging from rational design-based understanding of relationships between structure at the atomic/molecular level and performance. Precise structural characterization of these new nanomaterials, particularly in situ characterization under working conditions, is essential for establishing such structure−activity relationships and for guiding molecular designs of new nanomaterials.[1–4] Therefore, different complementary techniques such as X-ray absorption (XAS), Raman, and infrared spectroscopies have been used to investigate the local structure and ligand environment of nanometer sized materials.[5–7]

Catalyst development is one area in which nanomaterials have shown promise; these nanocatalysts can be comprised of single atoms, metal clusters, or particles composed entirely of molecules with a metal center and surrounding organic ligands. To date, most work has focused on the synthesis and characterization of metallic nanoclusters, which have demonstrated unique activity not observed in the bulk analogous materials. For example, supported gold nanoclusters display unique activity for CO oxidation[8–10] and Pd nanoparticles have shown high activity for NO reduction by CO.[11] Transition metal nanoparticles have also shown the ability to form carbon−carbon bonds.[12] However, there has been little research on nanoparticles composed entirely of transition metal complexes[13–16] even though it has been demonstrated that they may exhibit different properties than those of their bulk analogs. For instance, a vanadium phosphorus oxide (VPO) catalyst synthesized using precipitation with compressed antisolvent (PCA) technology and precipitated from CO_2 was more active in the oxidation of *n*-butane than the traditionally prepared catalyst and did not require as extensive a pretreatment process.[17]

Co(salen) [salen is bis(salicylaldehyde)ethylenediamine)] has been investigated for a wide range of applications including gas separation and storage[18] and as an oxidation catalyst in a wide variety of solvents.[19,20] Because it has been postulated that the first step in the oxidation is the binding of O_2 to the Co(salen),[21] a considerable amount of effort has been spent analyzing the properties of Co(salen)−dioxygen complexes.[22,23] It has been demonstrated that compared to Fe and Mn

* To whom correspondence should be addressed. E-mail: address: jguzman@ku.edu.
[†] Center for Environmentally Beneficial Catalysis and Department of Chemical and Petroleum Engineering, University of Kansas.
[‡] Department of Chemistry, University of Kansas.
[§] University of California, Irvine.

10.1021/jp803985b CCC: $40.75
Published on Web 07/23/2008

complexes, Co systems show potential as an O_2 absorbent from air.[18] We have shown recently that metal salen complexes can be processed into nanoparticles using PCA technology.[13] Our studies have shown that Co(salen) nanoparticles have rod-like structures and interact with diatomic compounds including dioxygen.[24] However, the dioxygen binding process is not well understood as a function of particle size or the structure(s) of the Co(salen) complexes within the nanoparticles. Therefore, conducting quantitative gas binding studies coupled with structural characterizations of the complexes would afford fundamental insights on the structure−function relationships between the precursor complexes and their corresponding nanoparticles.

A normally anticipated benefit of size reduction is an increase in the number of accessible reactive sites within the material. A comparison of the quantitative O_2 adsorption on the unprocessed, starting Co(salen) complex and processed nanomaterials revealed that the Co(salen) nanoparticles yielded an O_2 uptake capacity of 1.51 mmol of oxygen/g of nanoparticle; in contrast, the unprocessed Co(salen) complex displayed no measurable O_2 binding.[24] In the present work, we report an investigation of PCA-processed Co(salen) nanoparticles by complementary techniques such as infrared, Raman, X-ray absorption near edge structure (XANES) and extended X-ray absorption fine structure (EXAFS) spectroscopies, and X-ray diffraction (XRD) experiments before, during, and after interaction with O_2. The spectroscopic results show that the enhanced O_2 binding properties of Co(salen) nanoparticles are correlated to a distorted tetrahedral coordination geometry of the Co(salen) complexes within the nanoparticulates, a structure that is not observed in unprocessed samples that contain mainly dimers with square pyramidal geometry.

Experimental Section

Materials and Sample Preparation. Commercial Co(salen) and cobalt(II) acetate were purchased from Sigma-Aldrich and used as received. The commercial Co(salen) will be referred to as unprocessed Co(salen) in this manuscript. The UHP grade oxygen and helium used for the adsorption experiments were obtained from AGA and Praxair Inc., respectively. Labeled $^{18}O_2$ (99 atom % ^{18}O) was purchased from Icon Isotopes. Cobalt(III) acetate was synthesized following an established procedure.[25] The Co(salen) nanoparticles were prepared using the PCA technique using a vessel of 0.95 L and Graver filter (0.1 μm),[13] which can be described as a high pressure spray dryer where an organic solution of the metal complex is sprayed into carbon dioxide near its critical point. The dense CO_2 preferentially extracts the solvent from the spray causing supersaturation and particle formation. The nanoparticles were stored in an argon-filled drybox until they were used for testing.

Characterization by Single Crystal and Powder Diffraction. Powder X-ray diffraction (PXRD) experiments were performed using a Rigaku D/Max 2200PC Ultima III multipurpose powder diffractometer with graphite-monochromated Cu Kα radiation. X-rays were provided by a normal-focus sealed X-ray tube operated at 40 kV and 44 mA. Scans were taken with an increment size of 1.0° over a range of 2Θ from 5° to 70°.

The single-crystal diffraction data was collected on a Bruker SMART APEX CCD Single Crystal Diffraction System.[26] X-rays were provided by a fine-focus sealed X-ray tube operated at 50 kV and 30 mA. A full hemisphere of diffracted intensities (1850 10-s frames with a ω scan width of 0.30°) was measured for a single-domain specimen using graphite-monochromated Mo Kα radiation ($\lambda = 0.71073$ Å). The Bruker software package SHELXTL was used to solve the structure using "direct methods" techniques. All hydrogen atoms were located from a difference Fourier and included in the structural model as independent isotropic atoms whose parameters were allowed to vary in least-squares refinement cycles. All stages of weighted full-matrix least-squares refinement were conducted using F_o^2 data with the SHELXTL Version 6.10 software package.[27] Experimental details about the crystal structure determination are given in Supporting InformationTable 1. Further explanation on the data analysis and processing is reported in the Supporting Information.

Characterization by Quantitative Gas Adsorption. Quantitative dioxygen adsorption experiments were carried out by Micromeritics Analytical Services with an ASAP 2020. The sample mass was 0.0334 g and the adsorption was carried out at 299 K. Additional experimental details are presented elsewhere.[13,24]

IR Spectroscopy. A Bruker Tensor 27 spectrometer with a spectra resolution of 4 cm^{-1} was used to collect transmission IR data of the samples, which were pressed into self-supporting wafers and loaded into an in situ reactor/cell (In Situ Research Instruments, Inc. South Bend, IN) connected to a flow system that allowed recording of the data while the treatment gases flowed through and around the sample. IR spectra of adsorbate ligands were determined by subtracting the background spectrum before the treatment gas came in contact with the sample. Spectra characterizing the ligands present during O_2 adsorption were recorded under various temperature conditions. Each reported spectrum is the average of 128−512 scans. Infrared spectra for the isotopic labeling experiments were collected on a Varian Scimitar 800 series FTIR instrument.

Raman Spectroscopy. A SpectraPro SP-2356 imaging spectrograph (600/1200/2400 g/mm; Princeton Instruments−Acton; Acton, MA) equipped with a CCD camera (1,024 × 256 picels; Princeton Instruments−Acton; Acton, MA) was used to collect the Raman spectra. The 532.43 nm excitation source was provided by a 130 mW diode pulsed solid state laser (Snake Creek Lasers, Halstead, PA). The 1200 gr/mm gratings provided an instrumental resolution of 5.7 cm^{-1} (1.9 cm^{-1} per CCD pixel). The samples were prepared as KBr pellets.

X-ray Absorption Spectroscopy (XAS). XAS experiments were performed at beamline D04B−XAFS1 of the Brazilian Synchrotron Light Laboratory (LNLS) at Campinas, Brazil; and at beamline X19A of the National Synchrotron Light Source (NSLS) at Brookhaven National Laboratory (BNL), New York, US. The ring current at LNLS was 250−170 mA and at NSLS was 250−150 mA. The storage ring operated with an electron energy of 0.9 GeV at LNLS and 2.5 GeV at NSLS. The samples were characterized by XAS spectroscopy before and during O_2 binding experiments. Each powder sample was pressed into a wafer and the mass of the sample was selected to give an absorbance of about 2.5 at the Co K edge (7709 eV). After a sample had been pressed, it was loaded into a cell, which was then aligned in the X-ray beam. XAS data were recorded in transmission mode; a double-crystal Si(111) monochromator was used, being detuned 20−25% to minimize the effects of higher harmonics in the X-ray beam. Each sample was scanned at least four times, and the reported data for each sample correspond to the average of the four scans. No changes were detected between the first and last scan of any sample, confirming that the X-ray beam did not affect the samples.

EXAFS Data Analysis. Analysis of the EXAFS data was performed by using a difference file technique with experimen-

TABLE 1: Crystallographic Data Characterizing the Reference Compounds and Fourier Transform Ranges Used in the EXAFS Analysis[a]

		crystallographic data			Fourier transform	
reference compound	shell	N	R, Å	ref	Δk, Å^{-1}	Δr, Å
Co	Co−Co	12	2.50	29	1.00−20.00	0.00−8.00
Co(salen)	Co−O	4	1.87	28	1.00−20.00	0.00−8.00
Co(salen)	Co−N	4	1.83	28	1.00−20.00	0.00−8.00

[a] Notation: N, coordination number; R, distance between absorber and backscatterer atoms; Δk and Δr, the range intervals used in the Fourier transformation.

tally and theoretically determined reference files by using the software FEFF 7.0 and FEFF 8.0 (Table 1).[28,29] Details of the preparation of the reference files and data analysis procedures are presented elsewhere.[30,31] The data were analyzed with the software XDAP.[32] No attempt was made to account for the small atomic X-ray absorption fine structure (data obtained at low values of r, the distance between the absorber (Co) and backscatterer atoms) of the spectrum other than by application of standard background subtraction techniques. Iterative fitting was carried out until excellent agreement was attained between the calculated k^0-, k^1-, and k^2-weighted data (k is the photoelectron wave vector) and the postulated model. The maximum number of free parameters n in the analysis was determined by the Nyquist theorem,[33] $n = (2\Delta k\Delta r/\pi) + 1$, where, Δk and Δr, respectively, are the intervals in k and r used to fit the data. The accuracies are estimated to be as follows: coordination number N, ± 10% for Co−high-Z contributions and ± 20% for Co−low-Z contributions; distance R, ± 0.02 Å; Debye−Waller factor $\Delta\sigma^2$, ± 20%; and inner potential correction ΔE_0, ± 20%. The fitting ranges in both momentum space and real space were determined by the data quality. The quality of the fitting was confirmed by the values of fit diagnostic parameters, ϵ^2_ν (goodness of fit) and the variances between the data and the model prediction for the EXAFS function χ and the Fourier transform of χ (for k^0-, k^1-, and k^2-weighting of the data).

Results

Structural Differences between Unprocessed and Nanoparticle Co(salen). Initial comparisons between the unprocessed Co(salen) and nanoparticles prepared from PCA processing were carried out using scanning electron microscopy. As shown in Figure 1, the size and morphology of the nanoparticles are dramatically different compared to the unprocessed Co(salen), which is characterized by a plate-like morphology with particle sizes on the order of tens of microns. In contrast, the Co(salen) nanoparticle powder was composed of an agglomeration of rod-like structures with an average diameter of about 100 nm and submicron length. As reported previously,[24] the nanoparticles yielded a much larger surface area (14−18 m^2 g^{-1}) and total pore volume compared to negligible values of these properties for the unprocessed complex. These disparities are also manifest in an approximately 20% reduction in the true (skeletal) density of the nanoparticles compared to the (conventional) starting complex. To further investigate the differences between the two samples, powder XRD was carried out on both samples (Figure 2). These studies indicated that the two samples contain species with different solid-sate structures. A partial loss of long-range order for the nanoparticles relative to the unprocessed Co(salen) is indicated by the broader peaks and fewer of them at higher diffracting angles in the PXRD pattern for Co(salen) nanoparticles relative to the PXRD pattern for unprocessed Co(salen). The PXRD pattern for Co(salen) nanoparticles also contains (additional) peaks that are not present in the PXRD pattern for the unprocessed Co(salen).

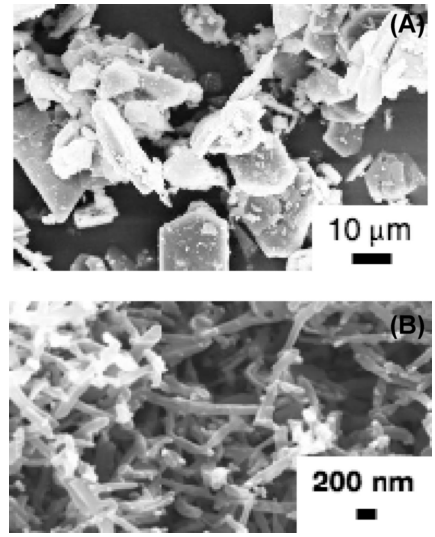

Figure 1. SEM images characterizing (A) unprocessed Co(salen) and (B) Co(salen) nanoparticles.

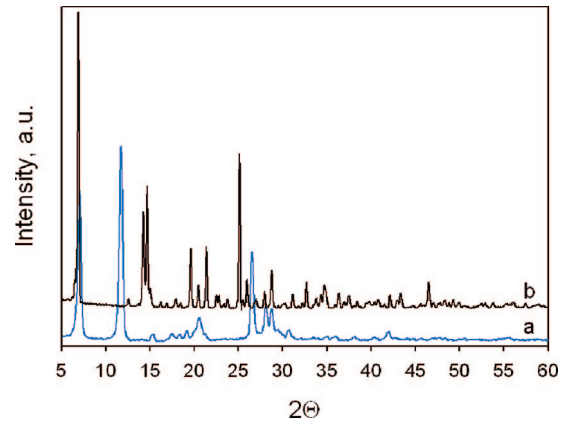

Figure 2. XRD data characterizing (a) Co(salen) nanoparticles and (b) unprocessed Co(salen).

Single crystal diffraction was also obtained for the unprocessed Co(salen). This sample was shown to be the same material previously characterized crystallographically at room temperature.[34,35] Analysis of the data indicates the presence of a dimer structure (Supporting Information Table 2). The coordination geometry around the cobalt ions was found to be five-coordinated with a tetragonally elongated square pyramidal coordination geometry and forming a dimer through a bridging oxygen atom. The "square" base consists of two oxygen donors and two nitrogen donors from a single salen ligand; the average Co−O and Co−N bond lengths are 1.907(2,14,2) and 1.883(2,1,2) Å, respectively (Supporting Information Table 2).[36] The apical coordination site is occupied by a salen oxygen from an adjacent Co(salen) moiety; this Co−O bond length is 2.212(2) Å. Each dimer therefore contains a four-membered −Co−O−Co−O− ring (Figure 3). Unfortunately, the Co(salen) nanoparticles did not

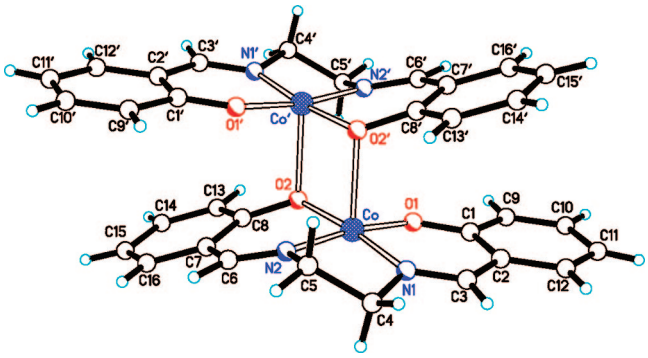

Figure 3. Perspective drawing for the dimeric $[Co(salen)]_2$ species present in single crystals of unprocessed Co(salen). Atoms labeled with a prime (′) are related to those labeled without a prime by the crystallographic inversion center located at (1/4, 1/4, 0) in the unit cell.

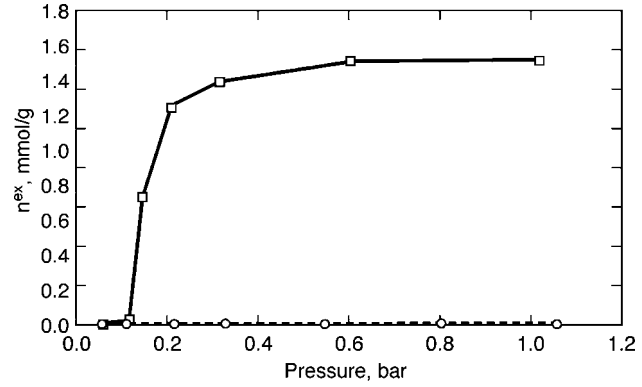

Figure 4. Quantitative O_2 adsorption results characterizing Co(salen) nanoparticles (continuous line) and conventional Co(salen) (dotted line) at 298 K.

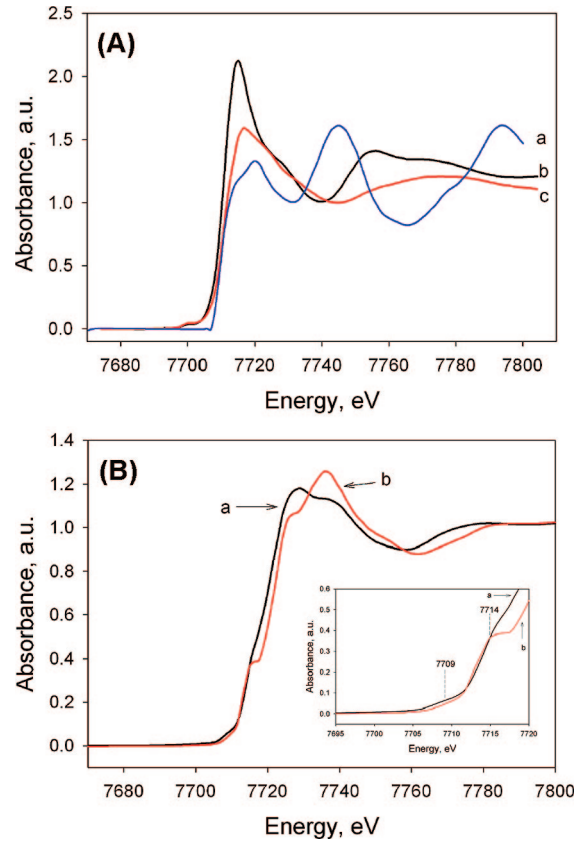

Figure 5. (A) XANES data characterizing Co standards: (a) Co foil; (b) $Co^{II}(CH_3COO)_2$; and (c) $Co^{III}(CH_3COO)_3$. The spectra were collected at room temperature in air. (B) XANES data characterizing (a) unprocessed Co(salen); and (b) Co(salen) nanoparticles. The insert shows the pre-edge region of the (a) unprocessed Co(salen); and (b) Co(salen) nanoparticles.

diffract well enough to produce an ample signal for routine single crystal diffraction. These results provide evidence of structural differences between the unprocessed starting material and the Co(salen) nanoparticles.

Dioxygen Adsorption on Unprocessed and Nanoparticle Co(salen). Quantitative dioxygen adsorption measurements were carried out to investigate the influence of the Co(salen) structure on binding performance. The Co(salen) nanoparticles displayed an uptake of 1.60 ± 0.08 mmol of oxygen/g of nanoparticle (Figure 4), a value that is in agreement with our previous measurements using a Rubotherm magnetic suspension balance.[24] Note that the unprocessed Co(salen) was also tested and found to display no measurable dioxygen uptake within the experimental detection limit of 0.01 mmol of oxygen/g of nanoparticle. A theroretical maximum of 1.54 mmol O_2 per gram of nanoparticle is predicted if dioxygen binds in a $Co:O_2$ ratio of 2:1.[24] These results suggest that in the Co(salen) nanoparticles each dioxygen molecule bridges between two Co(salen) complexes. Indeed, the nanomaterials display unique O_2 binding and NO disproportionation functionalities not seen with the commercial Co(salen). These unique properties and their catalytic application are detailed in a recently completed dissertation[37] and will be reported separately.

XANES Characterizing Unprocessed and Nanoparticle Co(salen). XANES provides information about the electron density around metal centers, and in our case it provided information on the oxidation state and site geometry around the cobalt centers. XANES data characterizing systems with known oxidation states and symmetries were obtained to provide a basis for interpretation of the features in the XANES spectra of our Co(salen) samples. Data were measured for Co^0 with Co foil, Co^{II} with $[Co^{II}(CH_3CO_2)_2]$, and Co^{III} with $[Co^{III}(CH_3CO_2)_3]$. The data characterizing the reference materials show that there is a prominent feature (white line) in the Co K edge spectra of Co^{III} centered at about 8 eV above the X-ray absorption edge (Figure 5A). Furthermore, the spectrum of Co^{III} shows a broad peak centered at 65 eV above the X-ray absorption edge. In contrast, the data characterizing Co^0 show a white line centered at 6 eV above the edge and two peaks at 36 and 85 eV above the edge.

XANES of the unprocessed and nanoparticulated Co(salen) samples show the presence of oxidized Co centers (Co^{II} and/or Co^{III}), as indicated by the lack of peaks at 36 and 85 eV above the X-ray absorption edge characteristic of metallic cobalt and by the white line centered at about approximately 7722 and 7723 eV for the unprocessed and the nanoparticulate Co(salen), respectively (Figure 5B). The XANES data characterizing the unprocessed Co(salen) sample contain two small pre-edge features, one at 7709 eV assigned to the $1s \rightarrow 3d$ transition, and a second at 7714 eV attributed to $1s \rightarrow 4p_z$ transitions.[38–41] The relatively small intensity of these two pre-edge features indicates that the cobalt center is centrosymmetric. In contrast, the XANES spectrum characterizing the Co(salen) nanoparticles show an intense pre-edge feature at 7715 eV, indicating a loss of centrosymmetry for the cobalt center.

EXAFS Characterizing Unprocessed and Nanoparticle Co(salen). EXAFS parameters characterizing both the unprocessed Co(salen) as well as the Co(salen) nanoparticles demonstrate structural differences between the two samples (Table 2).

TABLE 2: EXAFS Results Characterizing Nanoparticle and Unprocessed Co(salen) Samples at 298 K and a Pressure of 760 Torr[a]

	samples							
	Co(salen) unprocessed[b]				Co(salen) nanoparticles[c]			
absorber−backscatterer pair	N	R, Å	$10^3 \times \Delta\sigma^2$, Å^2	ΔE_0, eV	N	R, Å	$10^3 \times \Delta\sigma^2$, Å^2	ΔE_0, eV
Co−Co	0.5	2.92	14.10	13.4	—[d]	–	–	–
Co−O_s	2.0	1.91	0.25	15.0	1.8	1.90	1.31	4.2
Co−O_l	1.1	2.20	0.10	12.3	—[d]	–	–	–
Co−N	2.1	1.83	1.15	4.9	1.5	1.81	0.80	5.0

[a] Notation: N, coordination number; R, distance between absorber and backscatterer atoms; $\Delta\sigma^2$, Debye−Waller factor; ΔE_0, inner potential correction; O_s represents a short distance oxygen atom and O_l represents a long distance oxygen atom. Expected EXAFS errors: N, ± 10%; R, ± 0.02 Å; $\Delta\sigma^2$, ± 20%; ΔE_0, ± 20%. [b] The k and r ranges used in the data analysis for this sample are Δk = 3.61−14.99 Å^{-1} and Δr = 1.0−5.0 Å. %. [c] The k and r ranges used in the data analysis for this sample are Δk = 3.78−14.95 Å^{-1} and Δr = 1.0−5.0 Å. [d] Undetectable.

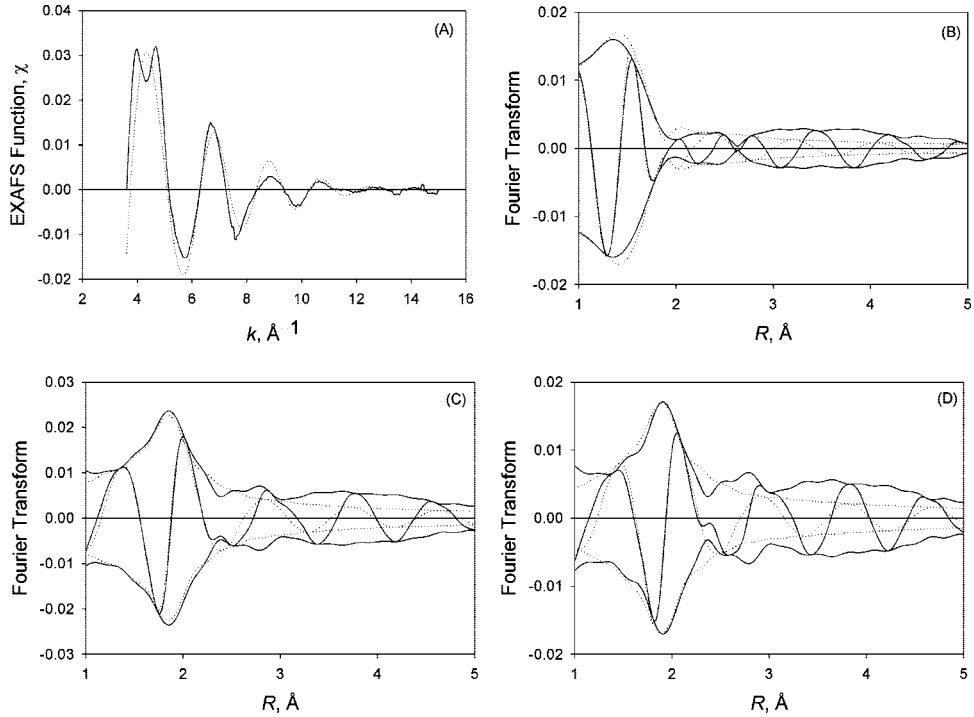

Figure 6. Results of EXAFS analysis characterizing the unprocessed Co(salen) sample at 298 K: (A) Experimental EXAFS function (solid line) and sum of the calculated Co−Co + Co−O + Co−N contributions (dotted line). (B) Imaginary part and magnitude of uncorrected Fourier Transform (k^0 weighted) of experimental EXAFS function (solid line) and sum of the calculated Co−Co + Co−O + Co−N contributions (dotted line). (C) Residual spectrum illustrating the Co−O_s contribution; imaginary part and magnitude of phase- and amplitude-corrected Fourier transform (k^1 weighted) of experimental data minus the calculated Co−Co, Co−N, and Co−O_l contribution (solid line) and calculated Co−O_s contribution (dotted line). (D) Residual spectrum illustrating the Co−N contribution; imaginary part and magnitude of phase- and amplitude-corrected Fourier transform (k^1 weighted) of experimental data minus the calculated Co−Co, Co−O_s, Co−O_l contributions (solid line) and calculated Co−N contribution (dotted line).

The data characterizing the unprocessed Co(salen) (Figure 6) indicate that on average two nitrogen atoms were bonded to the Co center at a Co−N distance of 1.83 Å. The cobalt ion was also coordinated to approximately two oxygen atoms at an average Co−O distance of 1.91 Å and to another oxygen atom at a longer distance of 2.20 Å. The data also show the presence of a long nonbonding Co−Co contribution (N = 0.5, where N is the coordination number of the contribution) at a distance of 2.92 Å. The results indicate that the unprocessed Co(salen) is a five-coordinated species, consistent with the single crystal X-ray diffraction data showing the presence of dimers. The EXAFS results characterizing the Co(salen) nanoparticles (Figure 7) indicate the presence of four-coordinated Co structures, as demonstrated by the Co−O (N = 1.8, R = 1.90 Å; where R is the distance from the absorber (Co) atom to the backscatterer atom) and Co−N (N = 1.5, R = 1.81 Å) contributions to the EXAFS spectrum. The EXAFS data characterizing both samples indicate the presence of intact Co(salen) structures, with no evidence of metallic cobalt clusters, confirmed by the lack of Co−Co contributions at bonding distances in the EXAFS spectra (Figure 8).

In Situ XANES During O_2 Adsorption. The XANES data collected during oxygen exposure of the unprocessed Co(salen) sample show virtually no changes with respect to the XANES spectrum characterizing the initial sample containing Co centers with a centrosymmetric geometry (Figure 9). The first derivative of the XANES data characterizing the Co(salen) complexes before and after 60 min of dioxygen exposure are shown in Figure 9B. The pre-edge features at 7709 and 7714 eV as well as the edge at 7722 eV show no change in intensity or position within the experimental error. These results are consistent with the microbalance data that showed no measurable O_2 uptake. In contrast, the XANES data collected during exposure of the Co(salen) nanoparticles to dioxygen show a gradual increase

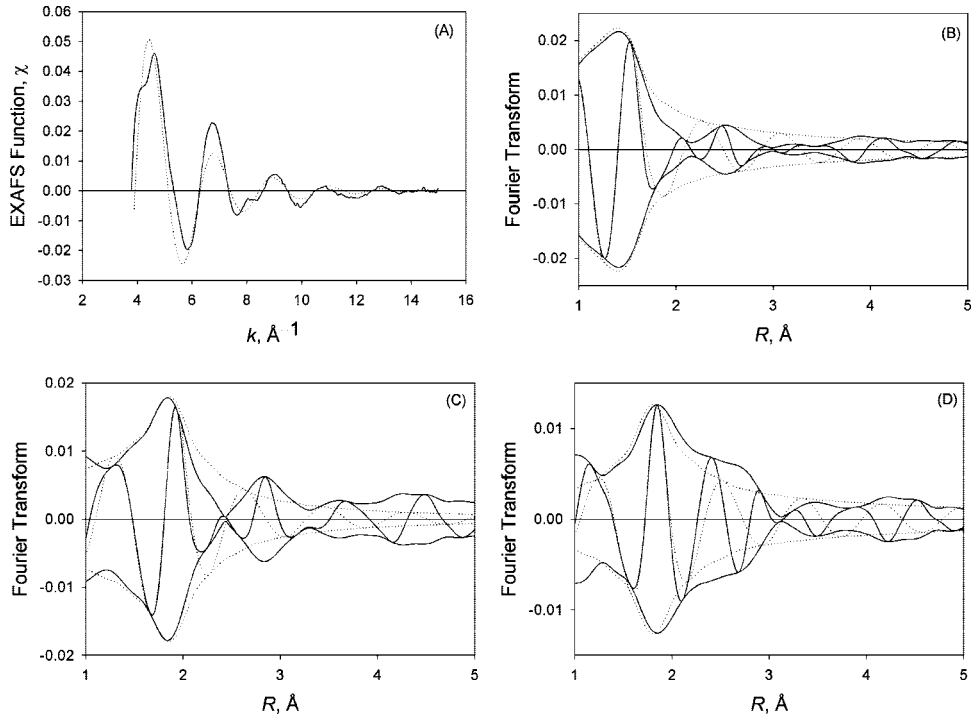

Figure 7. Results of EXAFS analysis characterizing the Co(salen) nanoparticle sample at 298 K: (A) Experimental EXAFS function (solid line) and sum of the calculated Co−O + Co−N contributions (dotted line). (B) Imaginary part and magnitude of uncorrected Fourier Transform (k^0 weighted) of experimental EXAFS function (solid line) and sum of the calculated Co−O + Co−N contributions (dotted line). (C) Residual spectrum illustrating the Co−O contribution; imaginary part and magnitude of phase- and amplitude-corrected Fourier transform (k^1 weighted) of experimental data minus the calculated Co−N contribution (solid line) and calculated Co−O contribution (dotted line). (D) Residual spectrum illustrating the Co−N contribution; imaginary part and magnitude of phase- and amplitude-corrected Fourier transform (k^1 weighted) of experimental data minus the calculated Co−O contributions (solid line) and calculated Co−N contribution (dotted line).

in intensity of the white line, indicating oxidation of the Co^{II} to Co^{III} (Figure 10). Furthermore, the first derivative of the XANES data characterizing the Co(salen) nanoparticles before dioxygen exposure and after 60 min of contact with dioxygen (Figure 10B) indicates a further loss of centrosymmetry as a consequence of the interaction of the Co center and oxygen, as indicated by decrease in intensity of the 7715 eV feature and the increase in the intensity at 7709 eV. The results are consistent with the coordination number of each cobalt center being increased by one, a result that agrees with findings from quantitative dioxygen uptake measurements as described above.

In Situ EXAFS During O_2 Adsorption. EXAFS data were determined for each sample in the presence of O_2 and after a subsequent treatment in Helium at 373 K for one hour. The samples were then cooled down to room temperature and analyzed. The EXAFS parameters characterizing the unprocessed Co(salen) complex during dioxygen exposure (Supporting Information Table 3) are undistinguishable from those characterizing the initial sample before any treatment (Table 2). These results are consistent with the lack of measurable O_2 uptake for this sample. There are two types of Co−O bonds that contribute to the EXAFS data: two relatively short Co−O bonds with an average distance of 1.91 Å and a one longer Co−O bond at 2.21 Å. The short Co−O bond length is most likely from the Co^{II} ion coordinated to a salen ligand, whereas the longer bond results from the bridging oxygen atom, which supports the presence of dimers in the sample. In addition, the parameters representing the Co−N contribution ($N = 2.0$, $R =$ 1.82 Å) are consistent with the bonding of the cobalt center to two nitrogen atoms from the salen ligand.

The EXAFS parameters (Table 3) characterizing the Co(salen) nanoparticles after exposure to O_2 at 298 K support the idea that each cobalt center has one additional oxygen-based ligand that distorts the centrosymmetry of the Co(salen) complex. The Co−O contribution to the EXAFS spectrum indicates that on average three oxygen atoms ($N = 2.9$) were bonded to the Co center at a distance of 1.90 Å. The increase in coordination number from 2.0 in the untreated sample to 2.9 in those treated with dioxygen supports the formation of a five-coordinate species, which is expected for Co(salen)(O_2) species. The Co−N contribution characterizing the Co(salen) nanoparticles is consistent with the retention of two coordinated salen nitrogen atoms ($N = 1.9$) at a distance of 1.80 Å (Figure 8).

The EXAFS data agree with our previously reported dioxygen uptake measurements that showed reversible O_2 binding to the Co(salen) nanoparticles.[24] In the samples exposed to He after oxygen exposure, the analysis of the EXAFS spectrum shows that two oxygen atom donors are coordinated to the cobalt center with an average Co−O bond distance of 1.90 Å. These values are statistically the same as those found for the Co(salen) nanoparticles analyzed before O_2 uptake (Table 2). Similarly, the Co−N contribution to the EXAFS spectrum for the sample after desorption in He ($N = 1.5$, $R = 1.82$ Å) is close to that found in the initially prepared Co(salen) sample. Taken together, these data show that the discrete four-coordinate Co(salen) complexes are present in the nanoparticles after treating with helium and the heating cycle, indicating a reversion back to the original coordination geometry found in the untreated samples. Furthermore, these structural data provide evidence for the stability of the Co(salen) complexes within the nanoparticles during the adsorption−desorption cycle.

In Situ FTIR Spectroscopy During O_2 Adsorption. Fourier transform infrared spectra were also collected on the nanoparticles to investigate changes in the ligand environment around the Co(salen) complexes before and after dioxygen exposure. Consistent with the quantitative O_2 uptake and XAS results,

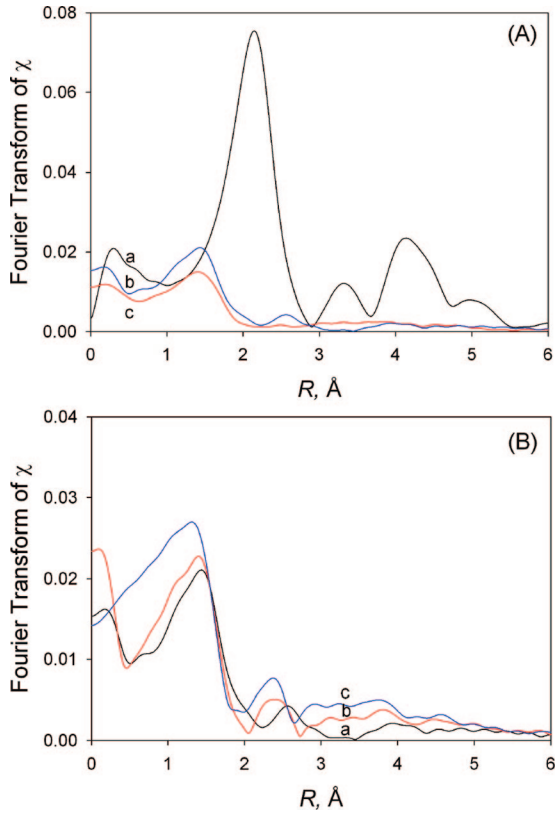

Figure 8. EXAFS results characterizing the magnitude of the phase- and amplitude-corrected Fourier transform (k^3-weighted) of the raw data illustrating (A) the lack of Co−Co contribution in (b) Co(salen) nanoparticles and (c) unprocessed Co(salen) (the spectrum of Co foil (a) is included for comparison); and (B) the increasing Co−O first-shell coordination numbers of the Co(salen) nanoparticles (a) before any O_2 treatment, (b) after treatment with O_2 for 1 h at 298 K, and (c) after treatment with O_2 for 24+ h at 298 K.

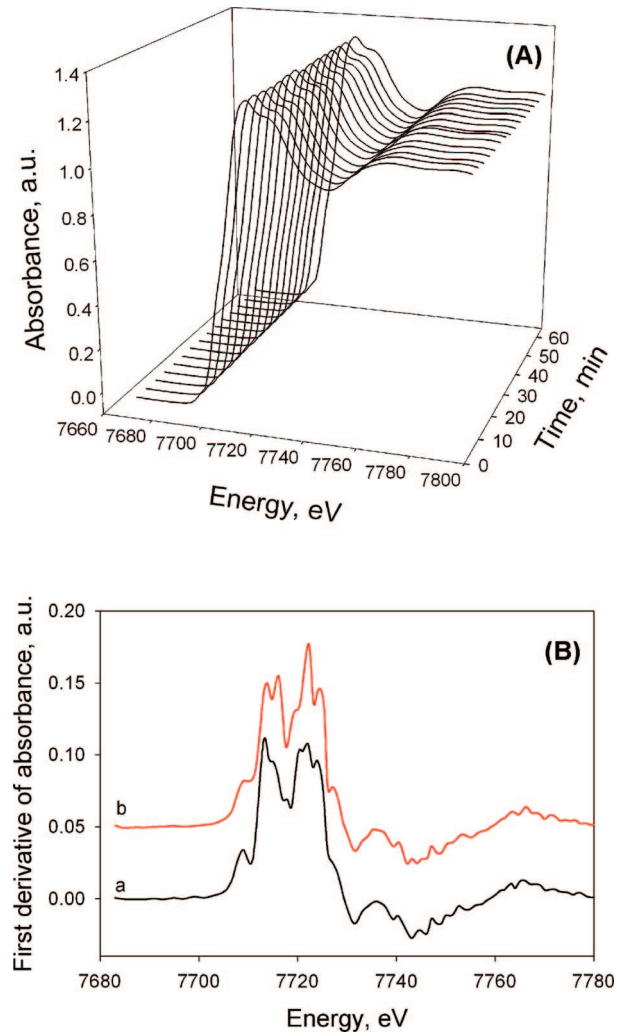

Figure 9. Time-resolved XANES data characterizing unprocessed Co(salen) in contact with O_2. (A) Transient data during exposure with O_2 at 298 K and (B) first derivative of the XANES spectra characterizing: (a) the initial sample and (b) after 1 h with O_2 at 298 K.

the unprocessed Co(salen) did not show any measurable changes in its vibrational properties upon exposure to dioxygen at 298 K (Figure 11A). In contrast, treating Co(salen) nanoparticles with dioxygen at 298 K produced new vibrational bands at 1630, 1550, 1272, 1553, and 1055 cm^{-1} (Figure 11B). The new bands observed in the spectrum increase in intensity as a function of dioxygen contact time, as illustrated for the band at 1272 cm^{-1} (Supporting Information Figure 1). Additionally, peaks at 1604 and 1309 cm^{-1} decrease in intensity after O_2 exposure while bands at 1467 and 1448 cm^{-1} increase in intensity. Finally, two bands shift upon exposure to O_2: the peak at 748 cm^{-1} shifts to 754 cm^{-1} and that observed at 727 cm^{-1} shifts to 733 cm^{-1}.

Raman Spectroscopy Characterizing O_2 Adsorption. Raman spectra were also collected on the nanoparticles to characterize the dioxygen interaction before and after exposure. The unprocessed Co(salen) did not show any measurable changes in its vibrational properties upon dioxygen exposure at 298 K (Supporting Information Figure S2), which is consistent with the quantitative O_2 uptake and XAS results. When the Co(salen) nanoparticles were exposed to dioxygen at 298 K, new vibrational bands appeared at 368, 547, 1046, and 1090 cm^{-1}. In addition, the intensities of these new vibrational bands decrease after purging the oxygenated samples with N_2 (Figure 12A). Three of these peak shift to lower energy upon treating the Co(salen) nanoparticles with $^{18}O_2$ (Figure 12B). In particular, the peak at 1046 cm^{-1} shifts to 986 cm^{-1}, which is predicted for a harmonic O—O oscillator ($\nu(^{16}O-^{16}O)/\nu(^{18}O-^{18}O)$ = 1.061; calcd 1.061). Furthermore, the 1090 cm^{-1} shifts to 1015 cm^{-1} with $^{18}O_2$ ($\nu(^{16}O-^{16}O)/\nu(^{18}O-^{18}O)$ = 1.074; calcd 1.060) and the band at 547 cm^{-1} goes to 530 ($\nu(Co-^{16}O)/\nu(Co-^{18}O)$ = 1.032; calcd 1.046).

Discussion

Evidence of Five-Coordinated Octahedral Dimers of Unprocessed Co(salen). The EXAFS, XANES, and XRD data provide evidence that the unprocessed Co(salen) is composed of dimers in which one salen oxygen atom of each salen ligand forms a bridge between two four-coordinate cobalt metals. Our single-crystal X-ray structural results are consistent with those reported by Bruckner et al.[34] and Delasi et al.[35] who found that Co(salen) can form similar dimers in the crystalline phase. The EXAFS and single crystal X-ray diffraction results show that each Co center has square pyramidal coordination geometry. The salen ligand binds as expected to the Co^{II} ions, forming two Co−O and Co−N bonds that defined the square plane. The primary coordination sphere of each cobalt ion is completed by an oxygen atom (O2 or O2′) of a neighboring salen ligand, forming Co−O2 bonds that are significantly longer than those in the square plane. The EXAFS data identified this Co−O contribution at a distance of 2.20 Å, which is in excellent agreement with the single crystal X-ray diffraction data that showed a Co−O2 bond distance of 2.212(2) Å. The net result

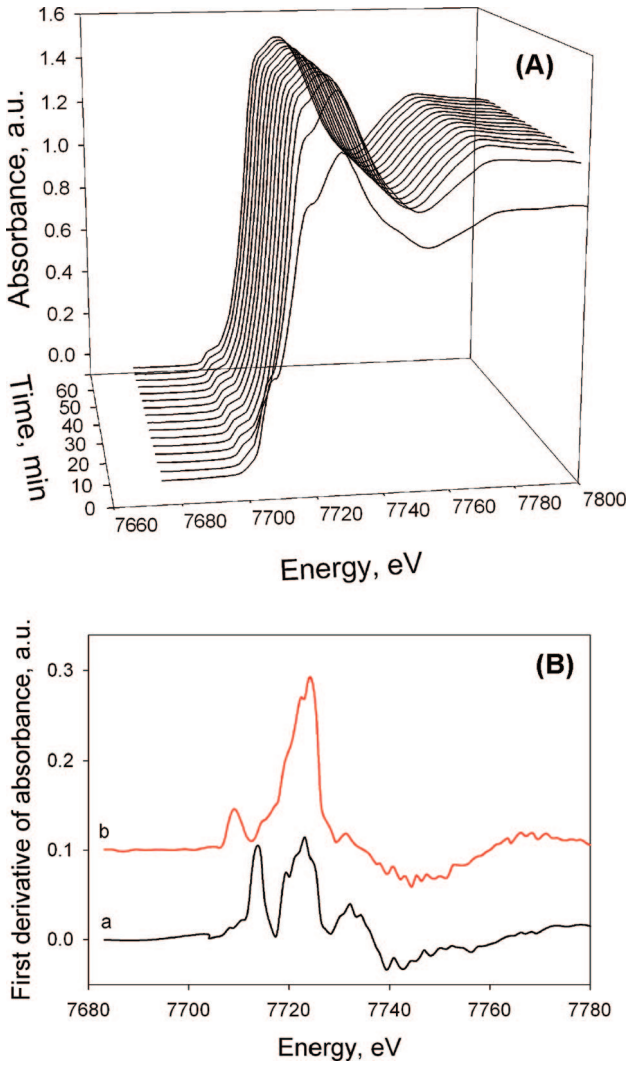

Figure 10. Time-resolved XANES data characterizing Co(salen) nanoparticles in contact with O_2. (A) Transient data during exposure with O_2 at 298 K and (B) first derivative of the XANES spectra characterizing: (a) the initial sample and (b) after 1 h with O_2 at 298 K.

is a dimeric structure that is supported by bridging oxygen atoms between the two cobalt centers.

Further structural information of the unprocessed Co(salen) is provided by the XANES data demonstrating that the Co center has a centrosymmetric geometry as indicated by the absence of a strong pre-edge in the XANES data (Figure 5) at approximately 7709 eV. This signal is characteristic of the 1s → 3d transition, which only arises from mixing between the 3d and 4p orbitals in noncentrosymmetry systems.[38–41] The absence of this transition would occur in complexes with either square-planar coordination geometry or a dimeric structure as found by X-ray diffraction (Figure 3) for unprocessed Co(salen) because both have centrosymmetric symmetry. The observed dimer structure produces two Co(salen) molecules that are stacked next to each other, leaving little space for the binding of additional molecules, including dioxygen. It has been proposed that this type of Co(salen) species is inactive toward oxygen adsorption because the close stacking of the complexes in the dimers prevents O_2 diffusion[42,43] Consistent with this hypothesis, the results reported herein show that the unprocessed Co(salen) species does not display any measurable O_2 uptake at room temperature.

Evidence of Four-Coordinated Distorted Tetrahedral Complexes within the Co(salen) Nanoparticles. While the unprocessed Co(salen) is a dimer in the solid state, it has been shown that it can form monomeric complexes when dissolved in solution.[42] In the PCA process, the nucleation and precipitation are so rapid that the monomeric form of the species is preserved during the recrystallization step. For example, it has been demonstrated through several examples that recrystallization in *sc*CO_2 fluid media can separate different polymorphs of compounds such as carbamazepine, salmeterol xinafoate, sulfathizole, and flunisolide.[44–47] The referenced investigations by York at al.[44,45,47] report that processing in *sc*CO_2 also forms certain polymorphs not observed using conventional crystallization techniques. Evidence of a nondimeric structure in the processed Co(salen) nanoparticles is found in the EXAFS data (Table 2) showing that the Co centers are four-coordinated, in which the Co atom is surrounded on average by two oxygen and two nitrogen atoms at a distance of 1.90 and 1.81 Å, respectively. These metrical results confirm that the Co(salen) complex remains intact after processing with CO_2. The Co−O and Co−N bond distances are not dramatically affected by the precipitation process as they are similar to those found in the unprocessed Co(salen) species ($R_{Co-O(1)}$ = 1.869(5) Å; $R_{Co-O(2)}$ = 1.835(4) Å; $R_{Co-N(1)}$ = 1.864(5) Å; and $R_{Co-N(2)}$ = 1.829(5) Å).[28] In addition, no other significant contributions were found in the EXAFS spectrum. Therefore, the fifth Co−O coordination detected in the unprocessed Co(salen) sample with a long distance of 2.2 Å is absent in the Co(salen) nanoparticles.

Although the complexes in the unprocessed and processed Co(salen) samples have similar bond lengths, the arrangement of the ligands around the cobalt ions is substantially different. Our data suggest that the Co(salen) complexes in the nanoparticle are not square planar, but rather have a distorted tetrahedral structure. The XANES data support this proposition. Figure 5 shows the XANES data characterizing the Co(salen) nanoparticles before exposure to O_2. The presence of an intense pre-edge peak at 7715 eV in the Co K edge is attributed to 1s → $4p_z$ transitions that are forbidden in a centrosymmetric geometry, but allowed in species with tetrahedral coordination geometry.[38] The presence of such an intense pre-edge feature at 7715 eV in the Co(salen) nanoparticles is indicative of the distorted tetrahedral coordination of the Co center. Other Co(salen) systems have been reported with distorted tetradedral structures; for instance, Eichhorn reported a strongly distorted tetrahedral framework for a Co(salen) complex when it is bonded to flavonolate.[48,49] We propose that the distorted tetrahedral geometry of the Co(salen) complexes within the nanoparticles makes for more accessible sites for O_2 binding, which contributes, in part, to the observed functional differences between processed and unprocessed Co(salen).

Influence of the Structural Differences During O_2 Uptake on Co(salen). The dioxygen uptake by the nanoparticulated Co(salen) is 1.60 mmol of oxygen per gram of nanoparticles, a value that is consistent with one O_2 molecule per two Co(salen) complexes. There have been several reports, including those with Co(salen),[43] that shown dioxygen binding to metal ions via a 1,2-μ-peroxo bridge—a binding mode that is consistent with these uptake results. Our structural results provide further support for this binding mode. The XANES results showed that upon exposure to O_2, the Co(salen) complexes within the nanoparticle are oxidized from Co^{II} to Co^{III}, a result that is consistent with dioxygen being reduced to a bridging peroxo moiety. Moreover, EXAFS results on O_2 treated nanoparticles indicated an increase in coordination number of the Co

TABLE 3: EXAFS Results Characterizing Co(salen) Nanoparticles Treated in O_2 and Subsequently Treated in He at 298 K and a Pressure of 760 Torr[a]

	treatment gas							
	O_2[b]				He after O_2[c]			
absorber−backscatterer pair	N	R, Å	$10^3 \times \Delta\sigma^2$, Å^2	ΔE_0, eV	N	R, Å	$10^3 \times \Delta\sigma^2$, Å^2	ΔE_0, eV
Co−Co	—[d]	–	–	–	—[d]	–	–	–
Co−O_s	2.9	1.90	0.10	12.5	1.8	1.90	1.31	4.2
Co−O_l	—[d]	–	–	–	—[d]	–	–	–
Co−N	1.9	1.80	0.50	5.10	1.5	1.82	0.80	5.0

[a] Notation: N, coordination number; R, distance between absorber and backscatterer atoms; $\Delta\sigma^2$, Debye−Waller factor; ΔE_0, inner potential correction. O_s represents a short distance oxygen atom and O_l represents a long distance oxygen atom. Expected EXAFS errors: N, ± 10%; R, ± 0.02 Å; $\Delta\sigma^2$, ± 20%; ΔE_0, ± 20%. [b] The k and r ranges used in the data analysis for this sample are Δk = 3.64−14.95 Å^{-1} and Δr = 1.0−5.0 Å. %. [c] The k and r ranges used in the data analysis for this sample are Δk = 3.76−15.51 Å^{-1} and Δr = 1.0−5.0 Å. [d] Undetectable.

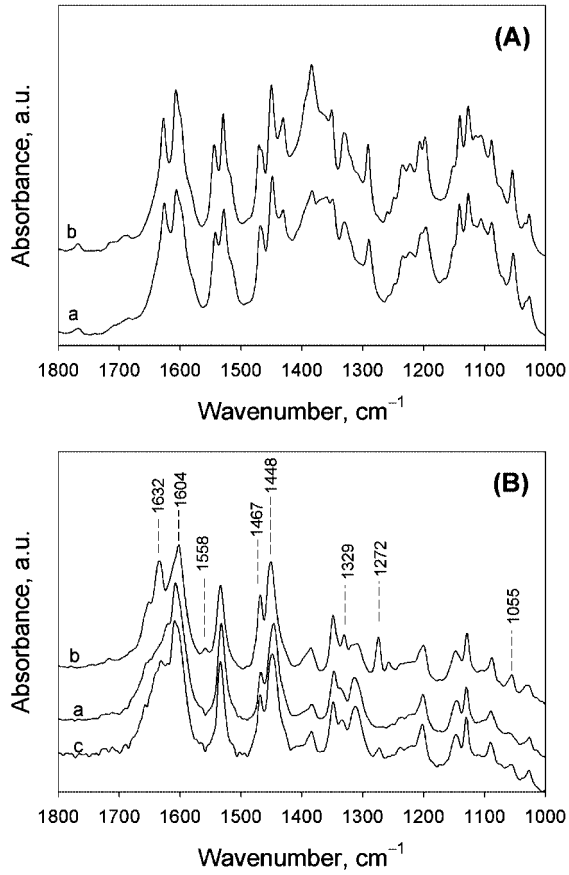

Figure 11. Infrared spectra characterizing the fingerprint region (1800−1000 cm^{-1}) of the (A) unprocessed Co(salen) sample (a) before any treatment and (b) after 38 min in flowing O_2 at 298 K and (B) Co(salen) nanoparticles (a) before any treatment, (b) after 38 min in flowing O_2 at 298 K, and (c) after subsequent treatment in He at 353 K for 60 min.

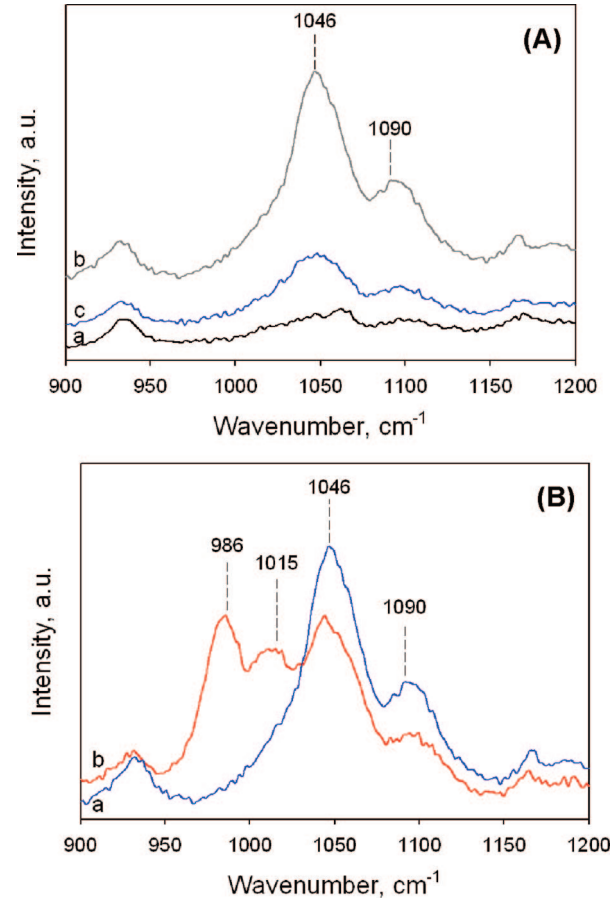

Figure 12. Raman spectra characterizing the ν(O−O) band of (A) the Co(salen) nanoparticles (a) before any treatment, (b) after flowing O_2 at 298 K, and (c) after subsequent treatment in N_2 at 298 K and the (B) Co(salen) nanoparticles (a) after treatment with $^{16}O_2$ at 298 K and (b) after treatment with $^{18}O_2$ at 298 K.

complexes from four to five compared to the original, untreated samples. Analysis of the EXAFS data found an additional Co−O contribution to the EXAFS spectrum, but we could not differentiate the Co−O bond distances between those arising from cobalt coordination to the salen ligand or dioxygen. Nevertheless, it provides average Co−O bond distances that are consistent with structural results derived from X-ray diffraction studies on a Co(salen)(pyridine) complex after O_2 adsorption.[50]

The vibrational results, specifically the Raman experiments, support the premise that dioxygen is binding to the cobalt complexes within the nanoparticles. The vibrational band at 1046 cm^{-1} is in the region normally associated with bridging peroxo ligands to cobalt complexes.[42,43] Moreover, we assign the band at 547 cm^{-1} to the Co−O symmetric stretches.[43]

The EXAFS data also demonstrated that the dioxygen uptake by Co(salen) nanoparticles is a reversible process. After an O_2 pulse, helium was flowed through the sample during a heating cycle to desorb the bound O_2.[24] The data showed that the Co−O coordination decreases to 1.8, a value matching that of the original sample before the O_2 exposure. Furthermore, the Co−N bond contribution also matches that of the original sample and provides further evidence that the Co(salen) is structurally stable during the adsorption−desorption cycle. Gentle heating in flowing He was also found to desorb the O_2 as was observed in the FTIR data shown in Figure 11B. Note that we found no changes in the data of comparable experiments with unprocessed Co(salen).

Conclusion

Co(salen) nanoparticles were prepared by the PCA technique using compressed CO_2. The structure and ligand environment of Co(salen) nanoparticles and unprocessed Co(salen) have been determined by the combined application of XRD experiments and infrared, XANES, and EXAFS spectroscopies before, during, and after interaction with O_2. Unprocessed Co(salen) particles with square-pyramidal coordination geometry that form dimers displayed no measurable binding for O_2 at room temperature. In contrast, the data indicate that the Co(salen) nanoparticles are composed of mononuclear Co(salen) complexes with distorted tetrahedral geometry, which exhibit enhanced O_2 uptake. Several pieces of complementary evidence of dioxygen uptake by the Co(salen) nanoparticles were noted, including the increase in the coordination number of the oxygenated nanoparticle that corresponds to the additional binding of a oxygen-based ligand and the oxidation of the cobalt centers from Co^{II} to Co^{III} upon exposure to dioxygen. The results provide evidence that the enhanced O_2 binding properties of Co(salen) nanoparticles are related to the unique distorted tetrahedral geometry, which is not observed in the unprocessed samples. The results presented here provide new fundamental insights into the relationship between active center structure and properties in new molecule-based nanomaterials.

Acknowledgment. This work was supported by the National Science Foundation (NSF-EEC 0310689). We acknowledge the Laboratorio Nacional de Luz Sincrotron (LNLS) in Campinas, which is operated by ABTLuS for the Department of Science and Technology in Brazil, for access to beam time in beam line D04B-XAS and the National Synchrotron Light Source (NSLS) at Brookhaven National Laboratory (BNL) in New York, which is supported by the U.S. Department of Energy, for access to beam time in beam line X19A.

Supporting Information Available: Details of crystal structure data analysis, crystallographic, EXAFS, FTIR, and Raman data of the unprocessed Co(salen). This material is available free of charge via the Internet at http://pubs.acs.org.

References and Notes

(1) Dahl, J. A.; Maddux, B. L. S.; Hutchison, J. E. *Chem. Rev.* **2007**, *107*, 2228.
(2) Kung, H. H.; Kung, M. C. *Appl. Catal. A* **2003**, *246*, 193.
(3) Bell, A. T. *Science* **2003**, *299*, 1688.
(4) de Meijere, A.; Hopf, H. *Chem. Rev.* **2006**, *106*, 4785.
(5) Gomez, R.; Solla-Gullon, J.; Perez, J. M.; Aldaz, A. *J. Raman Spectrosc.* **2005**, *36*, 613.
(6) Rioux, R. M.; Hoefelmeyer, J. D.; Grass, M.; Song, H.; Niesz, K.; Yang, P.; Somorjai, G. A. *Langmuir* **2008**, *24*, 198.
(7) Fierro-Gonzalez, J. C.; Kuba, S.; Hao, Y.; Gates, B. C. *J. Phys. Chem. B* **2006**, *110*, 13326.
(8) Haruta, M.; Tsubota, S.; Kobayashi, T.; Kageyama, H.; Genet, M. J.; Delmon, B. *J. Catal.* **1993**, *144*, 175.
(9) Valden, M.; Lai, X.; Goodman, D. W. *Science* **1998**, *281*, 1647.
(10) Guzman, J.; Gates, B. C. *J. Am. Chem. Soc.* **2004**, *126*, 2672.
(11) Judai, K.; Abbet, S.; Worz, A. S.; Heiz, U.; Henry, C. R. *J. Am. Chem. Soc.* **2004**, *126*, 2732.
(12) Manas, M. M.; Pleixats, R. *Acc. Chem. Res.* **2003**, *36*, 638.
(13) Johnson, C. A.; Sharma, S.; Subramaniam, B.; Borovik, A. S. *J. Am. Chem. Soc.* **2005**, *127*, 9698.
(14) Subramaniam, B.; Borovik, A. S.; Johnson, C.; Sharma, S. U.S. Patent application 20070134338, 2007.
(15) Wang, Z.; Ho, K. J.; Medforth, C. J.; Shelnutt, J. A. *Adv. Mater.* **2006**, *18*, 2557.
(16) Liu, B.; Qian, D.-J.; Chen, M.; Wakayama, T.; Nakamura, C.; Miyake, J. *Chem. Commun.* **2006**, 3175.
(17) Hutchings, G.; Bartley, J.; Webster, J.; Lopez-Sanchez, J.; Gilbert, D.; Keily, C.; Carley, A.; Howdle, S.; Sajip, S.; Caldarelli, S.; Rhodes, C.; Volta, J.; Poliakoff, M. *J. Catal.* **2001**, *197*, 232.
(18) Li, G. Q.; Govind, R. *Ind. Eng. Chem. Res.* **1994**, *33*, 755.
(19) Ming, W.; Musie, G. T.; Busch, D. H.; Subramaniam, B. *J. Am. Chem. Soc.* **2002**, *124*, 2513.
(20) Kervinen, K.; Korpi, H.; Mesu, J. G.; Soulimani, F.; Repo, T.; Rieger, B.; Leskelae, M.; Weckhuysen, B. M. *Eur. J. Inorg. Chem.* **2005**, *13*, 2591.
(21) Corden, B. B.; Drago, R. S.; Perito, R. P. *J. Am. Chem. Soc.* **1985**, *107*, 2903.
(22) Niederhoffer, E. C.; Timmons, J. H.; Martell, A. E. *Chem. Rev.* **1984**, *84*, 137.
(23) Norman, J. A.; Pez, G. P.; Roberts, D. A. In *Oxygen Complexes and Oxygen Activation by Transition Metals*; A. E. Martell, D. T. Sawyer, Eds.; Plenum Press: New York, **1988**; pp 107−125.
(24) Johnson, C. A.; Ottiger, S.; Pini, R.; Gorman, E.; Nguyen, J. G.; Munson, E.; Mazzotti, M.; Borovik, A. S.; Subramaniam, B. submitted.
(25) Koubek, E.; Edwards, J. O. *J. Inorg. Nucl. Chem.* **1963**, *25*, 1401.
(26) SMART Software Reference Manual (1998). Bruker-AXS, 5465 E. Cheryl Parkway, Madison, WI 53711−5373 USA.
(27) G. M. Sheldrick (2000). SHELXTL Version 6.10 Reference Manual. Bruker-AXS, 5465 E. Cheryl Parkway, Madison, WI 53711−5373 USA.
(28) Schaefer, W. P.; Marsh, R. E. *Acta Crystallogr.* **1969**, *B25*, 1675.
(29) Wycoff, R. W. G., Ed. In *Crystal Structures*, 2nd ed.; Wiley: New York, 1963; Vol. 1.
(30) Kirlin, P. S.; van Zon, J. B. A. D.; Koningsberger, D. C.; Gates, B. C. *J. Chem. Phys.* **1990**, *94*, 8439.
(31) van Zon, J. B. A. D.; Koningsberger, D. C.; van't Blik; H. F. J.; Sayers, D. E. *J. Chem. Phys.* **1985**, *82*, 5742.
(32) Vaarkamp, M.; Linders, J. C.; Koningsberger, D. C. *Physica B* **1995**, *209*, 159.
(33) Lytle, F. W.; Sayers, D. E.; Stern, E. A. *Physica B* **1989**, *158*, 701.
(34) Bruckner, S.; Calligaris, M.; Nardin, G.; Randaccio, L. *Acta Crystallogr.* **1969**, *B25*, 1671.
(35) DeIasi, R.; Holt, S. L.; Post, B. *Inorg. Chem.* **1971**, *10*, 1498.
(36) The first number in parentheses following an average value of an interatomic distance is the root-mean-square estimated standard deviation of an individual datum. The second number is the average deviation from the average value, respectively. The third number represents the number of individual measurements that were included in the average value.
(37) Johnson, C. A., Ph.D. Dissertation, University of Kansas, **2008**.
(38) Padden, K. M.; Krebs, J. F.; Trafford, K. T.; Yap, G. A.; Rheingold, A. H.; Borovik, A. S.; Scarrow, R. C. *Chem. Mater.* **2001**, *13*, 4305.
(39) This assignment is made based on analogy to peaks found in square planar Ni^{II} complexes: Colpas, G. J.; Maroney, M. J.; Bagyinka, C.; Kumar, M.; Willis, W. S.; Suib, S. L.; Baidya, N.; Mascharak, P. K. *Inorg. Chem.* **1991**, *30*, 920.
(40) Padden, K. M.; Krebs, J. F.; MacBeth, C. E.; Scarrow, R. C.; Borovik, A. S. *J. Am. Chem. Soc.* **2001**, *123*, 1072.
(41) Vralstad, T.; Glomm, W. R.; Ronning, M.; Dathe, H.; Jentys, A.; Lercher, J. A.; Oye, G.; Stocker, M.; Sjoblom, J. *J. Phys. Chem. B* **2006**, *110*, 5386.
(42) Hester, R. E.; Nour, E. M. *J. Raman Spectrosc.* **1981**, *11*, 49.
(43) Suzuki, M.; Ishiguro, T.; Kozuka, M.; Nakamoto, K. *Inorg. Chem.* **1981**, *20*, 93.
(44) Daintree, L. S.; Kordikowski, A.; York, P. *Adv. Drug Del. Rev.* **2008**, *60*, 351.
(45) Tong, H. H. Y.; Shekunov, B. Y.; York, P.; Chow, A. H. L. *J. Pharm. Sci.* **2008**, *97*, 1025.
(46) Moribe, M.; Tozuda, Y.; Yamamoto, K. *Adv. Drug Del. Rev.* **2008**, *60*, 328.
(47) Edwards, A. D.; Shekunov, B. Y.; Kordikowski, A.; Forbes, R. T.; York, P. *J. Pharm. Sci.* **2001**, *90*, 1115.
(48) Eichhorn, E.; Rieker, A.; Speiser, B.; Stahl, H. *Inorg. Chem.* **1997**, *36*, 3307.
(49) Hiller, W.; Nishinaga, A.; Rieker, A. Z. *Naturforsch* **1992**, *47b*, 1185.
(50) Schaefer, W. P.; Huie, B. T.; Kurilla, M. G.; Ealick, S. E. *Inorg. Chem.* **1980**, *19*, 340.

JP803985B